

Dynamical transition to spontaneous scalarization in neutron stars: the massive scalar field scenario

Juan Carlos Degollado,^{1,*} Néstor Ortiz,^{2,†} and Marcelo Salgado^{2,‡}

¹*Instituto de Ciencias Físicas, Universidad Nacional Autónoma de México,
Apartado Postal 48-3, 62251, Cuernavaca, Morelos, México*

²*Instituto de Ciencias Nucleares, Universidad Nacional Autónoma de México,
Circuito Exterior C.U., A.P. 70-543, México D.F. 04510, México.*

We analyze numerically the dynamical transition to spontaneous scalarization in neutron stars in the framework of a scalar-tensor theory of gravity where the scalar field is free but massive, and it is coupled non minimally to gravity in the Jordan frame. We show that the quasi-static configuration of the star that settles after the transition can avoid the observational constraints imposed on the amount of scalarization by several observations in binary systems due to the presence of the mass term, which suppresses the range of the scalar field. We also study the impact of the scalar field mass on the total mass of the star relative to the massless scenario.

PACS numbers: 04.50.-h, 04.50.Kd, 04.20.Ex, 04.25.D-, 95.30.Sf

I. INTRODUCTION

Scalar-tensor theories of gravity (STT) are one of the simplest alternatives to Einstein's theory of general relativity (GR) (see Refs. [1, 2] for a review). These theories introduce a new fundamental (real-valued) scalar field, ϕ , apart from the metric tensor, g_{ab} , in the description of gravity. A prominent example of this kind of theories is the Jordan-Brans-Dicke theory [3–5], which has inspired a large amount of research during the past six decades or so, and provides a covariant mechanism to generate a variation of Newton's gravitational "constant" G in terms of the scalar field ϕ . This kind of variation, specially a cosmic temporal variation of G_{eff} , was proposed during the 1990's to explain an apparent spatial periodicity in the distribution of galaxies around our own galaxy [6, 7]. As a bonus, this concocted model accounted for the dark sector of the universe (in the large scale), at least at the background level, prior to the discovery of the current accelerated expansion of the universe via the observation of supernovae SNIa, and prior to the cosmic-microwave-background (CMB) evidence on the presence of a cosmological constant [8–10]. Later, STT were also analyzed more thoroughly in cosmological settings [11–14].

STT are usually formulated in two equivalent, but *philosophically* different fashions. One is the formulation in the so-called *Jordan frame* (JF), where the scalar field ϕ appears non minimally coupled (NMC) to gravity, but with no direct coupling to the matter sector, and therefore, test particles follow geodesics of the so-called *physical metric* or JF metric, and the corresponding energy-momentum tensor (EMT) of matter T_{ab} is conserved. The other formulation, the *Einstein-frame* (EF) or conformal frame representation of STT, is concerned with a scalar field $\tilde{\phi}$, related to ϕ , which couples minimally to a conformal metric \tilde{g}_{ab} , but non minimally to the corresponding EMT, \tilde{T}_{ab} (see the Appendix A). Under the latter formulation, test particles do not (in general) follow geodesics associated

with the conformal metric, and thus, its corresponding EMT is not conserved, in general. Both representations have their own advantages, but the underlying physical effects (at least at the classical as opposed to the quantum level) are independent of the frame employed in the analysis [15]. In this paper we will focus mainly on the JF formulation, although, for practical reasons, we use the EF metric in some numerical calculations, as described in Secs. III and V. An important feature of STT is that they have a well posed Cauchy (initial value) problem, notably, when formulated in the JF [16, 17].

From the phenomenological point of view, STT faces different challenges as basically any alternative to GR. The stringent bounds imposed by several local observations (*e.g.* solar system tests), as well as cosmological (*e.g.* the CMB) and astrophysical observations (*e.g.* binary systems, including binary pulsars) limit its possible deviations from GR due to the scalar field ϕ [18]. Surprisingly, the theoretical discovery of the phenomenon of *spontaneous scalarization* (SC) in neutron stars under the framework of STT, by Damour and Esposito-Farèse [19] in the early 1990's, predicted deviations from GR in the strong-gravity regime while avoiding local and cosmic bounds. This phenomenon is analogue of *spontaneous magnetization* in ferromagnets at low temperatures [20], in the sense that under certain conditions on the compactness of a neutron star, an energetically preferred configuration appears "suddenly" within the object, which is accompanied by the presence of a non trivial scalar field cloud around the star while keeping the total baryon number fixed. This scalar field is endowed with an *order parameter* termed *scalar charge*, analogue to *magnetization* in ferromagnets. The non trivial scalar field does not require sources (*i.e.* potentials) and vanishes asymptotically. This phenomenon is immune to solar system tests, and also to cosmological bounds, first because it does not appear around the sun due to its low compactness, and second, because it does not require a cosmological value, as the scalar field vanishes asymptotically.¹

*Electronic address: jcdegollado@icf.unam.mx

†Electronic address: nestor.ortiz@nucleares.unam.mx

‡Electronic address: marcelo@nucleares.unam.mx

¹ The *induced scalarization*, as opposed to *spontaneous scalarization*, corresponds to a phenomenon in compact objects where a background scalar field, *i.e.* a non-zero asymptotic value for ϕ , is present. In this case, one

The SC phenomenon is a non-perturbative effect [19] which in principle provides a new avenue for testing STT. In fact, STT also predicts a new polarization mode of gravitational waves (GWs), termed *breathing mode*, which leads to isotropic distortions of spacetime at the passage of GWs (even in the direction of propagation, like longitudinal waves do in matter) and which may be generated even in spherical symmetry. However, this does not occur in GR, where the predicted (transverse and traceless) GWs are sourced only by distributions of matter with quadrupole time-variations, and thus which deviate from spherical symmetry. Moreover, GWs predicted by GR distort the spacetime only in the directions orthogonal to the passage of waves under the form of two independent modes ($++$, $\times\times$). This feature has been corroborated systematically by the LIGO-VIRGO-KAGRA collaboration since 2014 [21], which has detected GW signals mainly sourced by the inspiraling and subsequent collision of binary black holes. Regarding the simplest scenarios within GR, and even in STT, black holes (BHs) do not admit *hair*, notably in the form of a scalar field. This feature is consistent with current GW observations, which do not show evidence of a scalar field, whose presence might distort the predicted GW patterns. However, the story is different with neutron stars (NSs). In principle, the dynamical transition to SC could lead to the presence of scalar GWs that might be detected directly by future observatories sensitive to the breathing mode, or indirectly by showing distortions in the patterns of the (usual) tensor modes of GWs [22]. The first numerical analysis showing that such scalar GWs could be emitted during the transition to SC was performed by Novak [23]. Moreover, he showed that such waves can be further emitted during the gravitational collapse of a scalarized NS into a BH [24]. Later, it was discovered that SC can also take place in boson stars [25, 26], and more recently, even in BHs in particular theoretical contexts. For a broad review on the phenomenon of SC for diverse compact objects and theories, see [27] and references therein.

Another, not less astonishing, consequence of the phenomenon of SC is that the maximum mass of NSs within STT can be larger than in GR [19, 28]. This might be put forward to explain the existence of recently observed NSs with masses larger than two solar masses [29–32], without the need of exotic or very stiff equations of state. Despite these remarkable predictions, STT may seem to conflict with observations in binary pulsars, and more generally in binary systems [20, 33–36].² These systems constrain the amount of scalarization in NSs since the presence of the scalar field can affect drastically their dynamics in a way that its effects should have been already observed, but this is not the case. Thus, such astro-

physical systems restrict the amplitude of the scalar field in scalarized NSs, as well as the coupling constant whose value controls the deviation of STT from GR. A vanishing NMC constant leads to a theory with a minimally coupled scalar field to gravity, which is of no relevance if the value of the scalar field vanishes cosmologically. Binary-system tests and the resulting bounds on STT rely strongly on the range of the scalar field. Since the phenomenon of SC was originally discovered in STT with a massless scalar field ϕ , which becomes long-ranged after the transition to SC takes place in the star, with an asymptotically falloff as $\sim 1/r$ from its center, $r = 0$, its effects can influence the companion in a binary system. Nevertheless, recent analysis by several authors [38–46] show that the SC phenomenon can appear also if one adds a mass term to the STT. The presence of that term results in a short-ranged scalar field (depending on the value of the mass μ) with an exponential decay of Yukawa-type, $\sim e^{-\mu r}/r$, away from the NS, which in turn, may avoid the bounds imposed by observed binary systems.

In a previous work [47], we performed a numerical analysis of the transition to SC in NSs using polytropic equations of state (EOS), similar to the one reported by Novak several years ago [24], except that we have considered a specific STT formulated in the JF with a NMC function quadratic in ϕ . Furthermore, we analyzed the effects of the NMC function on the final amplitude of the scalar field after the transition to SC, and confronted its value with current bounds imposed by the binary systems alluded above.

In this paper, we continue the analysis of Ref. [47] by adding a mass term, as in [38–46], and study the dynamical transition to SC, as well as the range of the scalar field as compared with the typical size of observed binary systems for different values of the field mass μ . We show that some of the observational bounds may be avoided even with large values of the NMC constant, provided that the scalar field mass is sufficiently large. The latter is, however, orders of magnitude smaller than the masses of particles (fundamental or composite) associated with the standard model of particle physics.

This paper is organized as follows. In Section II we specify a STT in the JF with a massive scalar field, and write down the corresponding field equations. We describe static, spherical NSs modeled by a perfect fluid and a polytropic EOS in Section III. In Section IV, we set initial data for the non linear dynamical transition to SC, which is described in Section V. We discuss our results in Section VI, and conclude in Section VII. We have crosschecked our numerical results using two different codes, one based on the JF [47], and one based on the EF [48], thus we summarize relations between the JF and EF in Appendix A. The evolution equations implemented in the latter case are provided in Appendix B. We use units such that the speed of light in vacuum, c , and Newton’s constant, G , are both set to one.

II. SCALAR TENSOR THEORY

We shall study a NMC scalar field within the framework of a STT in the JF, as described in [26, 49]. The action of the

has to take into account the bounds imposed on local observations, like the bounds on the post-Newtonian parameters in the solar system due to a non-zero effective Brans-Dicke parameter ω_{BD} , which has to be larger than $\sim 4 \times 10^4$ in order to avoid the observational bounds (see Sec. II). Nevertheless, in the spontaneous scalarization scenario, where $\phi \rightarrow 0$ asymptotically, $\omega_{BD} \rightarrow \infty$.

² A STT example with a massless, NMC scalar field evading pulsar-timing constraints is discussed in Ref. [37].

theory is given by

$$S[g_{ab}; \phi; \psi_m] = \int \left[\frac{f(\phi)}{2} R - \frac{1}{2} (\nabla\phi)^2 - V(\phi) \right] \sqrt{-g} d^4x + S_m[g_{ab}; \psi_m], \quad (1)$$

where $S_m[g_{ab}; \psi_m]$ represents the action for matter fields ψ_m (which for the problem at hand are taken as a perfect fluid), and $f(\phi)$ is a positive definite NMC function of the form $f(\phi) = (1 + \kappa\xi\phi^2)/\kappa$, where $\kappa = 8\pi$, and ξ is a positive, dimensionless constant that parametrizes deviations from GR. The scalar field potential $V(\phi)$ will be specified below.

Variation of the action (1) with respect to the metric yields field equations that can be recasted as effective Einstein field equations,

$$R_{ab} - \frac{1}{2} g_{ab} R = \kappa T_{ab}, \quad (2)$$

where the total EMT is $T_{ab} = (T_{ab}^{\text{fluid}} + T_{ab}^{\phi} + T_{ab}^f)/(\kappa f)$, where contributions from the fluid, scalar field, and function f , are respectively given by

$$T_{ab}^{\text{fluid}} = (\epsilon + p)u_a u_b + p g_{ab}, \quad (3)$$

$$T_{ab}^{\phi} = (\nabla_a \phi)(\nabla_b \phi) - g_{ab} \left[\frac{1}{2} (\nabla\phi)^2 + V(\phi) \right], \quad (4)$$

$$T_{ab}^f = \nabla_a (f' \nabla_b \phi) - g_{ab} \nabla_c (f' \nabla^c \phi), \quad (5)$$

where u^a is the fluid's 4-velocity, ϵ is the total energy-density in the rest frame of the fluid, and p is the pressure as measured in the same frame. Here, primes indicate derivatives with respect to the scalar field ϕ . The diffeomorphism invariance of STT leads to the conservation of the EMT of matter alone, $\nabla_a T_{\text{fluid}}^{ab} = 0$, which in turn provides the hydrodynamic equations for the fluid.

In this work, we focus on a potential for a massive, but otherwise free, scalar field of the form

$$V(\phi) = \frac{1}{2} \mu^2 \phi^2, \quad (6)$$

where μ is the mass associated with the scalar field particle. We consider this mass to be in the range $1.33673 \times 10^{-12} \text{ eV} \leq \mu \leq 1.06859 \times 10^{-10} \text{ eV}$. For convenience, we operate with a dimensionless mass μ/μ_c , where $\mu_c = 1.33573 \times 10^{-10} \text{ eV}$. Then, our interval becomes $0.01 \leq \mu/\mu_c \leq 0.8$ (see Table I). Moreover, to simplify the notation, we shall rename the dimensionless mass $\mu/\mu_c \rightarrow \mu$, except for Sec. VI.

Regarding the NMC constant ξ , although the constraints imposed by pulsars and binary systems yield the bound $\xi \leq 2.5$ for the massless model [33], here we consider two values for this parameter, $\xi = \{15, 30\}$, so to enhance the scalarization process and check that the mass term suppresses the range of the scalar field to the extent that the observational constraints are to be avoided. These results are discussed in Section VI.

Variation of the action (1) with respect to the scalar field ϕ gives the equation of motion

$$g^{ab} \nabla_a \nabla_b \phi + \frac{1}{2} f' R = V'. \quad (7)$$

TABLE I: Equivalence of dimensionless field mass μ/μ_c , denoted μ [adim].

μ [adim]	μ [eV]
0.1	1.33573×10^{-11}
0.2	2.67146×10^{-11}
0.3	4.00719×10^{-11}
0.4	5.34292×10^{-11}
0.5	6.67865×10^{-11}
0.6	8.01438×10^{-11}
0.7	9.35011×10^{-11}
0.8	1.06859×10^{-10}

In the particular case of $f \equiv 1/\kappa$, which in the current scenario corresponds to $\xi \equiv 0$, the theory reduces to Einstein's GR with a minimally coupled scalar field, and with ordinary matter fields. On the other hand, when $\phi \equiv 0$, the STT reduces to GR with a matter content as defined within S_m as part of the total action (1). The STT can be recasted into a Brans-Dicke (BD) type from the action (1) by defining a new scalar field $\Phi = f(\phi)$, and by performing the necessary steps so that the kinetic term for the scalar field Φ takes the desired form with a prefactor that includes a BD function $\omega_{BD}(\Phi)$ [16]. In the original BD theory, $\omega_{BD} = \text{const}$, which has to be of the order of 4×10^4 within the solar system in order to pass the usual tests [50]. This bound is important when the scalar field is nonzero within the solar system. However, here we will be concerned only with a non zero scalar field in the neighborhood of a NS that can be part of a binary system, which is otherwise far enough from the solar system to produce noticeable effects on it. In other words, we assume that if the SC phenomenon takes place in a NS, the latter is far enough from the solar system so that, for all practical purposes, the scalar field generated by the star has reached its asymptotic vanishing value in the neighborhood of the solar system, and thus the usual gravity tests remain unaffected as if $\omega_{BD} \rightarrow \infty$.

In the following, we study the consequences of the above theory on spherically symmetric NS models which, for simplicity, we describe in terms of a perfect fluid with a polytropic EOS (see Sec. III).

A. Scalarization in massive scalar-tensor gravity

While SC with a massive scalar field was studied in Refs. [38–46]³ with polytropic and other EOS, as far as we are aware, the dynamical transition from unscalarized to scalarized stars was not analyzed. Some of these works study static and spherically symmetric [39], or rotating NSs [40, 41] within a certain class of STT (different from the one we consider here) that supports a non trivial scalar field that vanishes asymptotically, and under the EF representation. In principle,

³ A review can be found in Sec. III-A-2 of Ref. [27].

those scalarized NSs are supposed to be precisely the result of an evolution like the one we analyze in this paper. Nevertheless, this is only so when the mass of the scalarized NS is below the maximum mass allowed in GR, *i.e.*, in the absence of the scalar field. By definition, a scalarized star corresponds to a preferred lower-energy (*i.e.* lower total mass) configuration than the unscalarized one with fixed total baryon mass. Thus, the final quasi-static configuration after scalarization ensue must have a mass lower than the mass of the initial, unscalarized star (the mass difference being radiated away in the form of scalar field). Therefore, scalarized NSs with masses larger than the maximum mass in GR cannot be the result of an evolution similar to the one considered here, but one of a much more complicated nature that requires perhaps some sort of accretion of scalar field by the star's surroundings, like the accretion of a similar scalar field of cosmic origin, for instance [47]. It would be very interesting in the future to devise a physical scenario that leads to the formation of “super” massive scalarized stars, *i.e.* stars with masses larger than the maximum mass models in GR.

III. STATIC STELLAR MODELS

Understanding the dynamical transition to scalarization requires first the analysis of static, equilibrium stellar models allowed within the STT under consideration. In Section IV, some of these stars will be taken as initial data for time evolution. Some others are expected to be the endpoint of evolution after a sufficiently long time.

Spherical star models in hydrostatic equilibrium are solutions of the structure equations that generalize the well known TOV equations from GR, with a perfect fluid given by the energy-momentum tensor of Eq. (3). Our numerical algorithm solves the structure equations in a formulation that combines the JF fluid variables, and the EF metric \tilde{g}_{ab} , which is related to the JF metric g_{ab} by the transformation $g_{ab} = a(\tilde{\phi})^2 \tilde{g}_{ab}$, with a function a that depends on the scalar field $\tilde{\phi}$, defined in the EF.⁴ The relation $\phi(\tilde{\phi})$, the specific function $a(\tilde{\phi})$, and the potential $\tilde{V}(\tilde{\phi})$, are all determined by the conformal transformation between frames, as we outline in Appendix A. The EF line element in Schwarzschild-like coordinates is given by

$$d\tilde{s}^2 = -\tilde{N}(r)^2 dt^2 + \tilde{A}(r)^2 dr^2 + r^2 (d\vartheta^2 + \sin^2 \vartheta d\varphi^2). \quad (8)$$

The static limit of the evolution system (B4)–(B22) results in the following structure equations,⁵

$$\begin{aligned} \frac{d\tilde{m}}{dr} &= 4\pi r^2 a^4 \epsilon + \frac{r}{2}(r - 2\tilde{m}) \left(\frac{d\tilde{\phi}}{dr} \right)^2 + \frac{r^2}{4} \tilde{V}(\tilde{\phi}), \\ \frac{d}{dr} \ln \tilde{N} &= \frac{4\pi r^2 a^4 p}{r - 2\tilde{m}} + \frac{r}{2} \left(\frac{d\tilde{\phi}}{dr} \right)^2 + \frac{\tilde{m}}{r(r - 2\tilde{m})} \end{aligned} \quad (9)$$

$$\begin{aligned} & - \frac{r^2}{4(r - 2\tilde{m})} \tilde{V}(\tilde{\phi}), \\ \frac{d^2 \tilde{\phi}}{dr^2} &= \frac{4\pi r a^4}{r - 2\tilde{m}} \left[\alpha(\epsilon - 3p) + r(\epsilon - p) \frac{d\tilde{\phi}}{dr} \right] \\ & - \left[\frac{2(r - \tilde{m}) - r^3 \tilde{V}(\tilde{\phi})/2}{r(r - 2\tilde{m})} \right] \frac{d\tilde{\phi}}{dr} + \frac{r}{4(r - 2\tilde{m})} \frac{d\tilde{V}}{d\tilde{\phi}}, \\ \frac{dp}{dr} &= -(\epsilon + p) \left[\frac{d}{dr} \ln \tilde{N} + \alpha \frac{d\tilde{\phi}}{dr} \right], \end{aligned} \quad (10)$$

with $\alpha := d \ln a(\tilde{\phi})/d\tilde{\phi}$, and the mass aspect function \tilde{m} defined through $\tilde{A}(r) = [1 - 2\tilde{m}(r)/r]^{-1/2}$. To close the above system of equations, we specify a polytropic EOS,

$$p(\rho) = K \rho_0 \left(\frac{\rho}{\rho_0} \right)^\gamma, \quad (13)$$

where K and γ are dimensionless constants, ρ is the fluid's baryon-mass density measured by comoving observers, and ρ_0 is a characteristic baryon-mass density given by $\rho_0 = m_b n_0$, where $m_b = 1.66 \times 10^{-24}$ g is the mean baryon mass, and $n_0 = 0.1 \text{ fm}^{-3}$ is the mean baryon-number nuclear density. The total energy-density in this case is given by

$$\epsilon(\rho) = \rho + \frac{p}{\gamma - 1}. \quad (14)$$

In this work, we consider a polytrope corresponding to a soft EOS, with $\gamma = 2.46$, and $K = 0.0093$. We notice, however, that other polytrope-parameter choices do not change our results qualitatively.

We employ a fourth-order Runge-Kutta algorithm to numerically integrate the structure equations (9)–(12), given a central baryon-mass density $\rho_c := \rho(0)$ [and thus a central pressure through Eq. (13)], an initial guess for the central scalar field $\tilde{\phi}_c := \tilde{\phi}(0)$, and regularity conditions $\tilde{m}(0) = 0$ and $d\tilde{\phi}/dr(0) = 0$. The stellar radius, R_s , is defined by the condition $p(R_s) = 0$ up to numerical tolerance. We iterate on $\tilde{\phi}_c$ until a solution is found such that $\tilde{\phi}(r) \rightarrow 0$ as r grows large. Our numerical domain typically consists of 5000 cells, and extends up to $\sim 20R_s$. Finally, the baryonic mass of a star model is given by

$$M_b = \int_0^{R_s} 4\pi r^2 \rho a(\tilde{\phi})^3 (1 - 2\tilde{m}/r)^{-1/2} dr. \quad (15)$$

Sequences of spherical, static NS models in the case of coupling constant $\xi = 15$ are shown in Fig. 1, where yellow lines correspond to solutions such that $\phi(r) = 0$, *i.e.* non scalarized solutions, which are also solutions of the GR equations of structure, thus sometimes referred to as “GR-like” solutions. In turn, green lines in Fig. 1 correspond to spontaneously scalarized solutions, meaning that they possess a non trivial $\phi(r)$ profile that can extend beyond the stellar surface. For coupling $\xi = 15$, scalarized solutions exist only up to values of $\mu \lesssim 0.5$. The bottom panel shows the central value of the scalar field, ϕ_c , as a function of baryonic mass M_b . In the case of $\xi = 15$, scalarized solutions feature no nodes in their $\phi(r)$

⁴ A similar Einstein-Jordan hybrid algorithm has been implemented in [51].

⁵ Under appropriate notation and convention changes, this set of equations reduces to the one in Ref. [40] in their static limit.

profile, in the sense that its sign never changes. Notice that branches of scalarized solutions—progressively darker green lines—become shorter as the scalar field mass μ increases. Also, notice that scalarized solutions reach a maximum baryonic mass larger than the GR-like solutions. Beyond this maximum, such stars are unstable to gravitational collapse. Most importantly, in the range where scalarized solutions exist, GR-like solutions are unstable to scalar field perturbations, and the endpoint of this instability is expected to be a scalarized solution of the same baryonic mass.

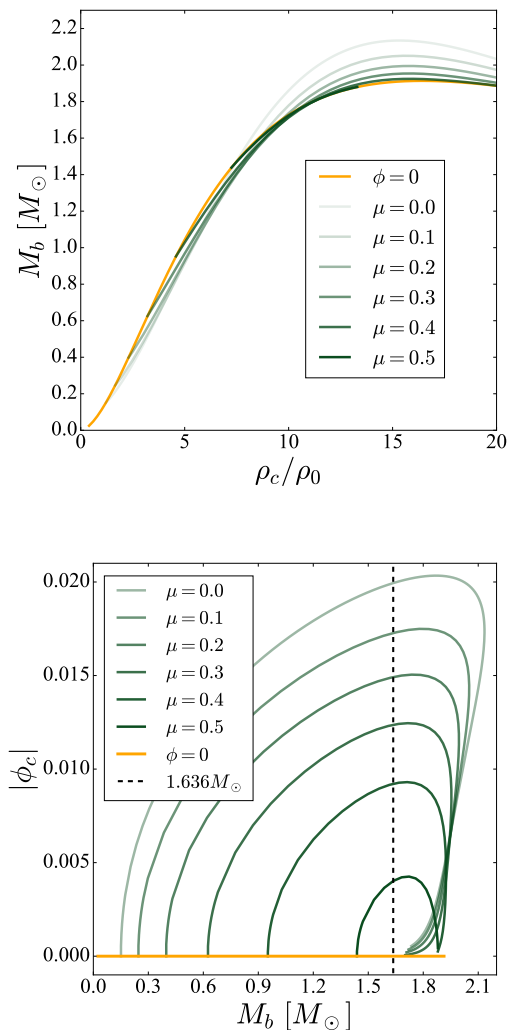


FIG. 1: Sequences of spherical, static stellar models in the case of coupling $\xi = 15$. Yellow lines correspond to non scalarized stars. Green lines correspond to branches of scalarized stars. Top panel: Baryon mass vs. central baryon density. Bottom panel: Central value of the scalar field vs. baryon mass. The vertical line corresponds to $M_b = 1.636 M_\odot$, which is the baryon mass of stars undergoing dynamical transition in Sec. V.

The case of coupling constant $\xi = 30$ features the same qualitative characteristics, as can be seen in Fig. 2. There

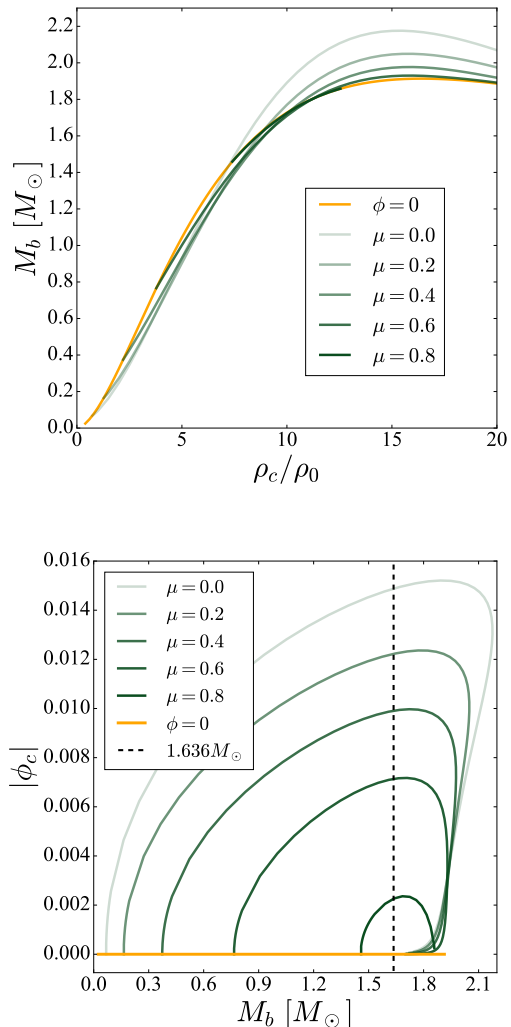


FIG. 2: Same as Fig. 1, for the case of coupling $\xi = 30$.

are two main differences though. First, in this case, spontaneously scalarized solutions do exist for $\mu > 0.5$, up to $\mu = 0.8$. Second, besides the 0-node scalarized solutions—green branches—, for $0 < \mu \lesssim 0.4$ there are scalarized solutions whose $\phi(r)$ profile features one node, meaning that it changes sign exactly once. The corresponding branches are shown in Fig. 3, where progressively blue lines correspond to progressively higher values of the mass μ . It is clear that the larger μ , the smaller the 1-node scalarized branch.

Several questions arise with respect to the existence of scalarized solutions with nodes in their $\phi(r)$ profile. Our numerical experience suggests that there is a critical value in the interval $15 < \xi < 30$ such that 1-node solutions show up, and then, the higher ξ , the more nodes appear in scalarized solutions. We have considered up to $\xi = 240$, and we have found up to 5 nodes in scalar field profiles. A capital question regarding scalarized solutions with nodes is about their stability to scalar field perturbations. In all of the cases we explored numerically, for a fixed baryonic mass M_b , the configu-

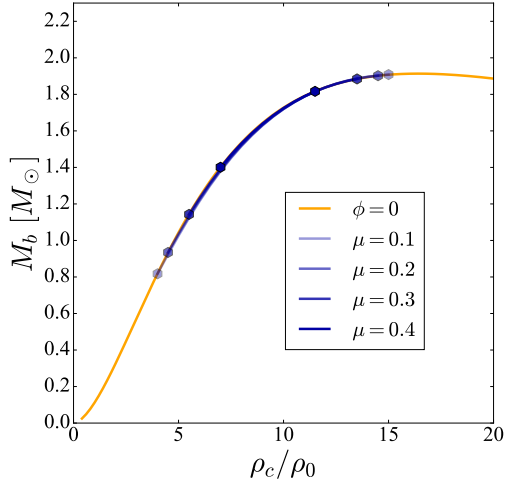


FIG. 3: Sequences of static, spherical stellar models in the case of $\xi = 30$. The yellow line corresponds to non scalarized stars. Blue branches correspond to scalarized stars with 1-node in their $\phi(r)$ profile. Dot marks indicate junctions to the non scalarized (yellow) sequence.

ration with no nodes always possesses a gravitational mass M smaller than any configuration with nodes. This suggests that 0-node stars are energetically favored over stars with nodes with the same baryonic mass. We confirm this expectation in Sec. V.

A more complete picture of what makes a 0-node scalarized star energetically preferred in terms of its gravitational mass M , is summarized in Fig. 4. It reveals that, for a given baryonic mass M_b and coupling ξ , a smaller field mass μ corresponds to smaller gravitational mass M . Most remarkably, for fixed M_b , and given μ and ξ , the non scalarized solution ($\phi(r) = 0$, red line) is the less energetically favored.

Figure 5 provides complementary aspects of static, scalarized solutions with no nodes. It shows that, for fixed coupling ξ , smaller field masses μ allow for scalarized stars to have a larger maximum gravitational mass M . The lack of points in the case of $\xi = 15$ for $\mu = \{0.6, 0.8\}$ is due to non existence of scalarized solutions beyond $\mu = 0.5$ for such a small ξ . Notably, keeping the EOS fixed, the maximum mass of scalarized solutions is always larger than the maximum mass allowed for non scalarized solutions, represented by a dashed line in Fig. 5.

IV. INITIAL DATA

Our main goal is to investigate the non-linear dynamical evolution from unscalarized NSs to stable, spherical, scalarized stars. This task requires numerical integration of the STT field equations, coupled to the scalar field equation of motion, as well as the hydrodynamical equations. Initial data for time evolution consist of non scalarized stars in hydrostatic equilib-

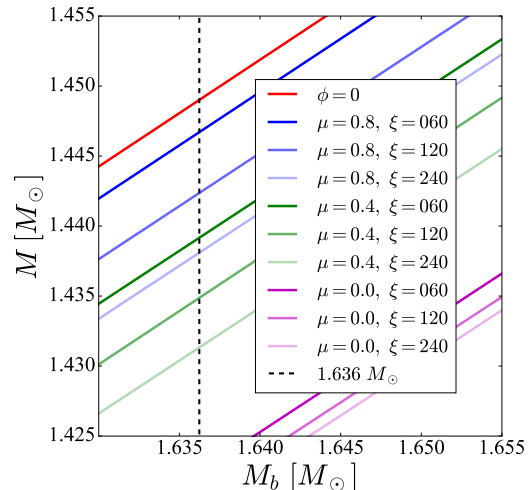


FIG. 4: Sequences of 0-node solutions. For any given baryonic mass M_b and fixed scalar field mass μ , the larger the coupling constant ξ , the lower the gravitational mass M . Likewise, for a given coupling ξ , the smaller the field mass μ , the lower the gravitational mass M . Therefore, smaller masses μ and larger couplings ξ lead to energetically preferred scalarized configurations. The vertical line indicates $M_b = 1.636M_\odot$, which is the baryon mass of stars undergoing dynamical transition in Sec. V

rium, *i.e.* $\phi = 0$ solutions of the structure equations (9)-(12), except for a small scalar field perturbation to trigger the transition of the star to the scalarized state. The initial configuration has a total mass below the maximum associated to the given EOS, and is stable against gravitational collapse into a black hole.

In view of the existence of scalarized solutions with an increasing number of nodes in their $\phi(r)$ profile as the coupling ξ gets larger, a natural question is whether or not slightly perturbed initial data are expected to evolve to a scalarized configuration with nodes. To give the answer, we focus on a scenario where scalarized 1-node solutions exist, concretely the case of $\xi = 30$, $M_b = 1.4M_\odot$, and $\mu = 0.3$. Figure 6 shows small portions of branches of static, equilibrium solutions in this case. The black line is a sequence of non scalarized stars, whereas blue and green lines correspond to 0- and 1-node sequences of scalarized stars, respectively. We consider the three existing solutions with baryon mass $M_b = 1.4M_\odot$. We label them with dots in Fig. 6, we show their ϕ -profiles in Fig. 7, and we report their parameters in Table II, where it is clear that the 0-node scalarized solution (blue dot) features the smallest gravitational mass M . Therefore, among the three solutions, the 0-node configuration is energetically favored, and it is thus expected to be the end state of time evolution if one takes initial data consisting on either the non scalarized solution (black dot), or the 1-node solution (green dot). In other words, since the dynamics ideally keeps the baryon mass constant, then starting either in the black or green dots of Fig. 6, a small perturbation will onset the scalar field in-

Index	Branch	Color in Fig. 6	ρ_c/ρ_0	$M [M_\odot]$	R [km]	$ \phi_c $
1	$\phi = 0$	Black	6.9851	1.26385	10.56	0
2	Scalarized, 0 nodes	Blue	7.5237	1.25722	10.53	0.0105
3	Scalarized, 1 node	Green	7.0579	1.26384	10.56	0.0029

TABLE II: Parameters of static, stellar models with fixed baryonic mass $M_b = 1.4M_\odot$, in the case of $\xi = 30$, $\mu = 0.3$. The scalarized solution with no nodes in its scalar-field profile minimizes the gravitational mass M , and is therefore energetically favored. Initial data consisting of solutions 1 or 3 are expected to evolve to a configuration consistent with solution 2.

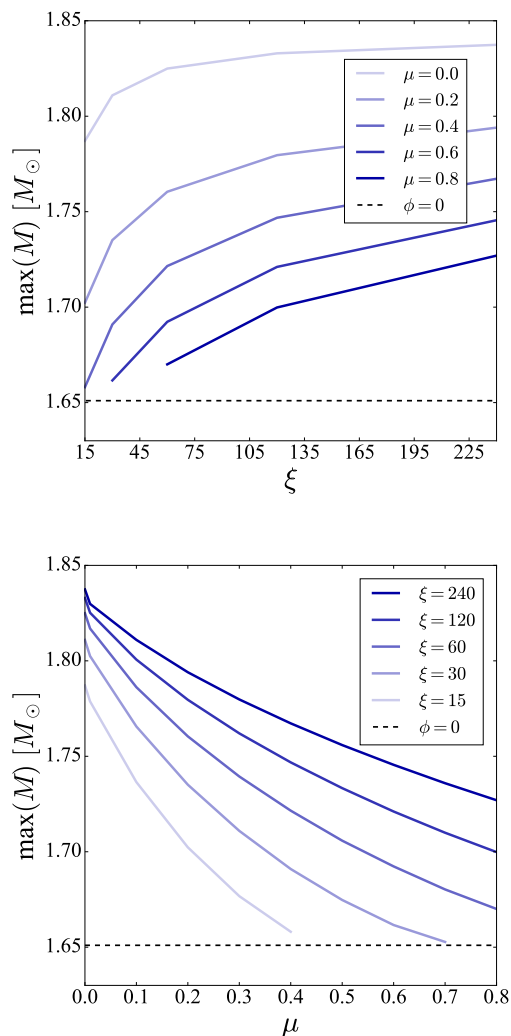


FIG. 5: Maximum of the gravitational mass M as a function of coupling constant ξ (top panel) and scalar field mass μ (bottom panel). Horizontal dashed lines indicate the maximum mass allowed for NSs in GR, for the EOS under consideration.

stability whose end-state after sufficiently long time should be consistent with the blue dot configuration. This expectation is confirmed in Sec. V, in particular Fig. 9. According to our numerical inspection, static, scalarized solutions with 0-nodes

are always energetically favored over solutions with nodes. This observation motivates the conjecture that the dynamical transition from non scalarized stars should always lead to scalarized solutions with 0-nodes. This conjecture holds in all of our numerical simulations of dynamical transition to scalarization, as reported in Sec. V. Static solutions chosen as

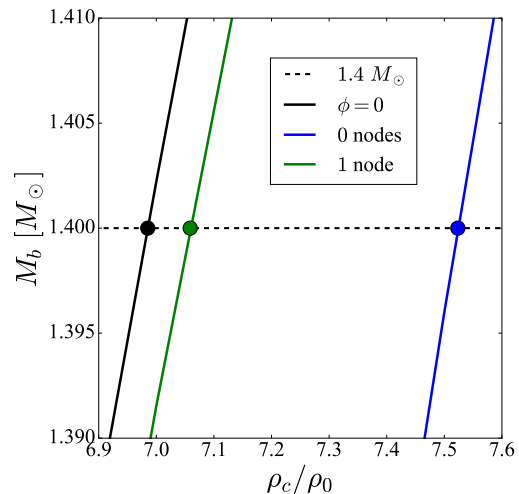


FIG. 6: Solid lines are small portions of NS sequences. Highlighted points correspond to $M_b = 1.4M_\odot$ stars in the case of $\xi = 30$, $\mu = 0.3$. The 0-node (blue point) configuration is energetically favored among the three highlighted stars, as can be read from Table II. Thus, if either the black or green points are taken as initial data, then time evolution drives them to a configuration consistent with the blue point configuration. This expectation is confirmed in Fig. 9. Our results show that 0-node configurations are always energetically favored over those with one or more nodes.

initial data for time evolution with different choices of μ have a central energy-density such that they lie in the branch *unstable* to scalar field perturbations. In other words, initial data are stable towards BH formation, but unstable towards transition to a scalarized state. We have arbitrarily chosen initial data with baryonic mass $M_b = 1.636M_\odot$, which corresponds to $\rho = 8.9245\rho_0$. These initial data are located in the yellow sequences of Figs. 1 and 2. Indeed, since the central value of the scalar field for initial data is $\phi_c = 0$, this corresponds to the intersection of the vertical dashed lines with horizon-

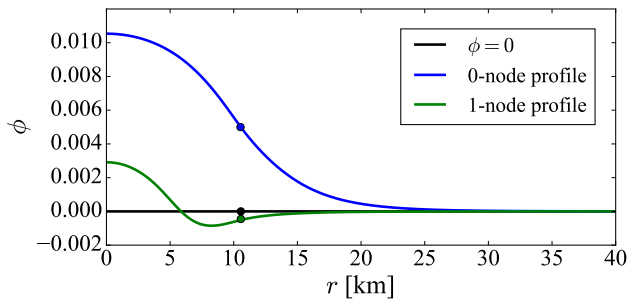


FIG. 7: Scalar-field radial profiles corresponding to the static solutions described in Table II, which are associated with colored circles in Fig. 6. The stellar radius in each case is indicated by small circles.

tal, yellow lines of bottom panels of Figs. 1 and 2. Time evolution drives the initial data to a scalarized configuration with $|\phi_c| \neq 0$, ideally conserving the baryon mass, thus corresponding in those two figures to the intersection of the vertical dashed line with a green curve, depending on the field mass μ . Another viewpoint of these initial data, in terms of the central value of their baryon-mass density ρ_c , is displayed in Fig. 8, which is a zoom-in to the top panels of Figs. 1 and 2. In both cases, $\xi = 15$ and $\xi = 30$, a black dot indicates initial data for time evolution. Horizontal, dashed lines correspond to constant baryon mass $M_b = 1.636 M_\odot$. Depending on the value of μ , colored marks indicate the expected final state of time evolution, which consist of 0-node scalarized stars. In the next section, concretely in Figs. 10 and 11, we show evidence that the dynamics brings initial data to the expected end-states.

V. DYNAMICAL TRANSITION TO SCALARIZED STATES

The dynamical process of scalarization is given by the solution in space and time of the effective Einstein-Scalar-field system (2)–(7), together with the hydrodynamic equations

$$\nabla_a T_{\text{fluid}}^{ab} = 0, \quad (16)$$

$$\nabla_a(\rho u^a) = 0. \quad (17)$$

We solve the whole system in spherical symmetry using two independent numerical codes.

The first code is also the one used to construct the static solutions of Sec. III. It evolves JF fluid variables, together with the EF metric functions and scalar field. The full evolution system can be found in Appendix B. The JF scalar field and metric components are recovered through the relations given in Appendix A. This code uses a finite-volume method with evolution equations written in conservative form. Details on the formalism, methods, boundary conditions, vacuum treatment, and convergence tests, can be found in Refs. [48] and [52].

The second code solves the evolution system entirely in the JF. It uses a modified BSSN formalism adapted to spherical

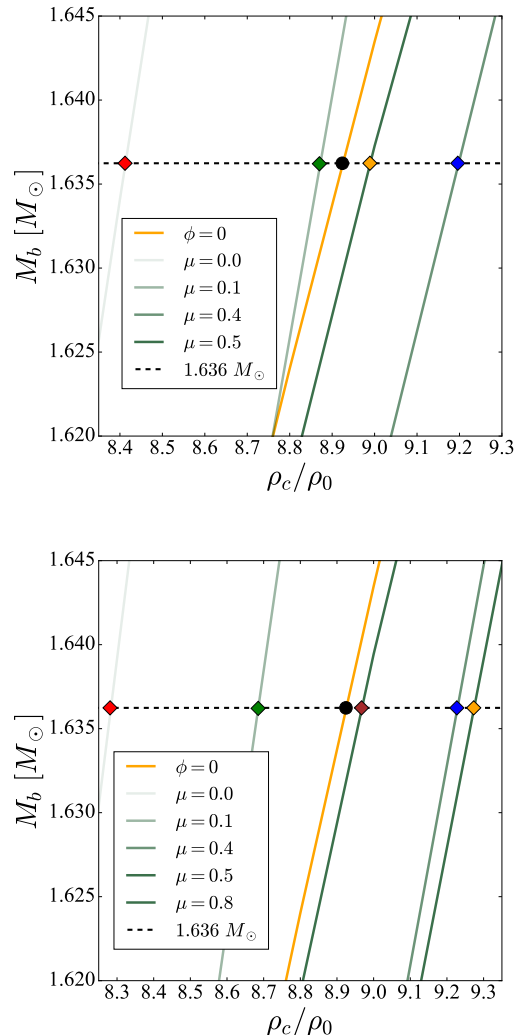


FIG. 8: Top panel: Zoom-in to star sequences of Fig. 1 ($\xi = 15$). Bottom panel: Zoom-in to sequences of Fig. 2 ($\xi = 30$). Black dots represent initial data for the time evolutions shown in Figs. 10 and 11, respectively. Colored diamonds indicate expected endpoints of those time evolutions.

coordinates like in [47], with the spatial metric given by

$$ds_3^2 = \psi(t, r)^4 \left[a(t, r) dr^2 + r^2 b(t, r) (d\vartheta^2 + \sin^2 \vartheta d\varphi^2) \right]. \quad (18)$$

This code was used in the past for an almost identical scenario, except that the scalar field was massless [47], and also when analyzing the dynamical transition to SC in spherically symmetric boson stars [26, 49]. A detailed description of the numerical method and variables employed during time evolution is given in Refs. [47, 53].

We have checked that, despite their different approaches and methods, the numerical codes that we used for analysis in the Einstein and Jordan frames, consistently return the same phenomenology, which further supports the equivalence between these two formulations of STT.

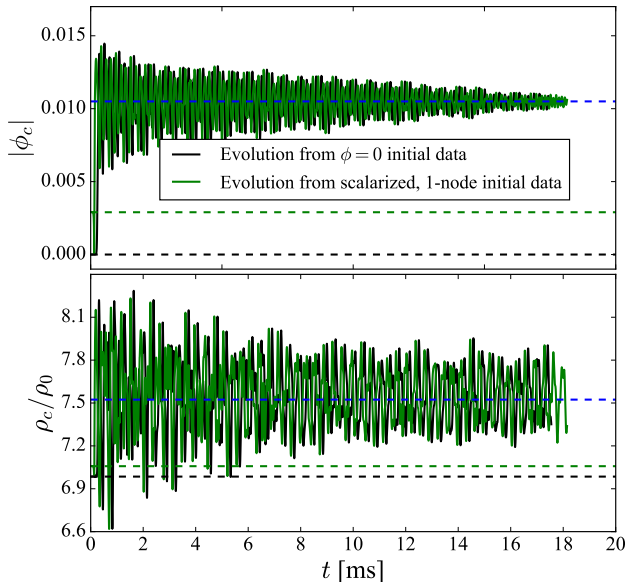


FIG. 9: Time evolution of the central value of the scalar field (top panel) and central value of baryon-mass density (bottom panel), in the case of $\xi = 30$, $\mu = 0.3$. The initial data corresponds to the black and green dots of Fig. 6. In both cases, time evolution drives the stars to the 0-node scalarized solution, consistent with the blue dot configuration in Fig. 6, which is energetically preferred, as described in Table II. Horizontal lines indicate values associated with the initial data and the expected endpoint of evolution.

Small numerical errors in the initial data construction are enough to onset the instability to scalar field perturbations. Time evolution then goes through an early phase of exponential growth, which should be comparable against predictions from linear perturbation theory.⁶ An alternative approach to the onset of the instability is to induce a quicker dynamical transition to scalarization by means of a gaussian perturbation into the scalar field, assuming staticity on the fluid and spacetime. This approach saves computing time, but misses details of the scalar-field exponential growth at early times, in the small-perturbation regime.

As a first dynamical experiment, we take initial data represented by the black and green dots of Fig. 6, which are associated with a static unscalarized star, and with 1-node static scalarized star, respectively. As anticipated in Sec. IV, once the scalar-field instabilities have triggered in both cases, and after sufficiently long times, the dynamical solution settles around the static scalarized 0-node solution represented by the blue dot in Fig. 6, because this is the energetically preferred

⁶ To our knowledge, linear perturbation equations are available only in the massless case. See, for example, Ref. [54].

configuration with the same baryon mass $M_b = 1.4M_\odot$. The expected behavior is confirmed in Fig. 9, where solid lines represent the time evolution of the central value of the scalar field, ϕ_c (top panel) and the central value of the baryon-mass density, ρ_c (bottom panel). In both panels, dashed horizontal lines indicate values associated with the static solutions represented by dots in Fig. 6, with the same color code. In both cases, the dynamical solution features a *quasi-static* configuration with a total mass lower than the initial one (*i.e.* the initial ADM mass minus some energy radiated away in the form of scalar field).

We now discuss the time evolution of non scalarized initial data indicated by black dots in Fig. 8, for different values of the scalar field mass μ . Figures 10 and 11 show the time evolution of the central values ϕ_c (top panel) and ρ_c (bottom panel), in the cases of $\xi = 15$ and $\xi = 30$, respectively. In every case, we see a dynamical transition from non scalarized to scalarized, quasi-static configurations which are consistent with the expected end-states indicated with color marks in Fig. 8. The values of ϕ_c and ρ_c for the expected end-states are indicated by horizontal, dashed lines of the corresponding color, and their parameters are summarized in Table III.

We find different, somewhat uneven, types of dynamical behavior, depending on the value of μ . Star oscillations are most strongly damped in the massless case, and the solution quickly settles around the expected scalarized configuration. This result is similar to those reported in Ref. [47]. We have run a case of small field mass, namely $\mu = 0.01$, and we find a dynamics very similar to the massless case—thus not shown—, suggesting that the limit of $\mu = 0$ is reached smoothly. However, the qualitative picture changes as we look at the case of $\mu = 0.1$, where damping is notably less aggressive, and long-lived oscillation modes get excited. A systematic study of oscillation spectra would be interesting, as well as comparison with predictions from linear perturbation theory, as reported in the massless case [54]. Such tasks are beyond the goals of this work.

Unlike the cases of $\mu = \{0, 0.1\}$, the oscillation amplitude for $\mu > 0.1$ is relatively larger for ϕ_c than ρ_c . These oscillations are of higher frequency, and they damp at different rates depending on the value of μ . Regardless of the details of the transient phase, in all cases we find strong indications that, at late times, the solutions tend to stabilize around quasi-static states corresponding to the expected scalarized configurations. In the particular case of $\xi = 15$ and $\mu = 0.8$, we notice that the initial data remains unscalarized and basically unchanged, in the sense that ϕ_c keeps oscillating around 0 with a tiny amplitude of the order of 10^{-10} , and ρ_c keeps oscillating around the initial central baryon-mass density. This behavior is also expected, and is consistent with the fact that there is no static, scalarized solution with baryon mass $M_b = 1.636$ in this case—see Sec. III.

An important effect of a massive scalar field during the scalarization process of a NS is that the amplitude and radial extent of the scalar field are suppressed as μ increases. This behavior can be appreciated from Fig. 12, which shows scalar field profiles corresponding to the static solutions expected to be the end-state of time evolutions displayed in

Color in Fig. 8	$\xi = 15$					$\xi = 30$				
	Red	Green	Blue	Orange	Brown	Red	Green	Blue	Orange	Brown
μ	0.0	0.1	0.4	0.5	0.8	0.0	0.1	0.4	0.5	0.8
ρ_c/ρ_0	8.4130	8.8678	9.1919	8.9893	8.9245	8.2781	8.6799	9.2225	9.2678	8.9667
$M [M_\odot]$	1.43006	1.43763	1.44820	1.44898	1.44897	1.42541	1.43253	1.44407	1.44624	1.44898
R [km]	10.94	10.57	10.19	10.20	10.21	11.07	10.74	10.28	10.21	10.21
$ \phi_c $	0.0199	0.0173	0.0092	0.0040	0.0	0.0149	0.0134	0.0099	0.0086	0.0023

TABLE III: Parameters of expected end-states of time evolution. They correspond to color marks in the bottom panel of Fig. 8. All of the configurations have $M_b = 1.636M_\odot$.

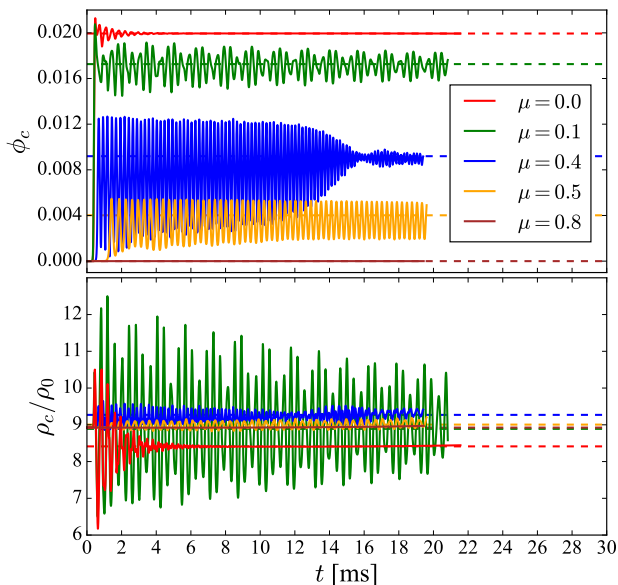


FIG. 10: Time evolution of the central value of the scalar field (top), and the central baryon-mass density (bottom), in the case of coupling $\xi = 15$.

Figs. 10 and 11. Notice how the scalar-field cloud hardly extends beyond the stellar surface—indicated by colored marks—in the cases of $\xi = 15$, $\mu = 0.5$, and $\xi = 30$, $\mu = 0.8$.

Another relevant quantity of the static, scalarized solutions is their total (ADM) mass M , which is plotted as a function of μ in Fig. 13, where the marks' color code is always consistent with previous figures. The smallest mass corresponds to the case of $\xi = 30$ and $\mu = 0$, which is the most scalarized configuration and therefore the one that differs the most from GR. As μ increases, all scalarized configurations tend to have the same total mass as in GR, since the scalar field is highly suppressed despite the relatively high values of the NMC constant ξ .

Although the spacetime of such spherical, static stars is asymptotically flat, it differs from the Schwarzschild solution outside the compact support of the fluid due to the scalar field contribution. This is manifested by the product of metric com-

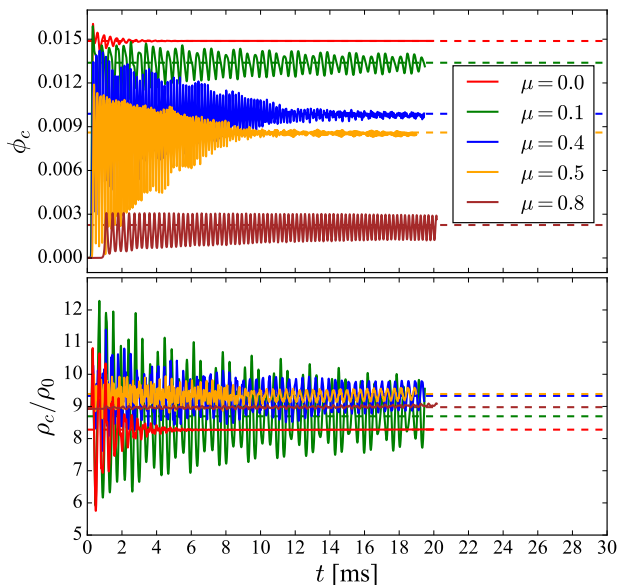


FIG. 11: Same as Fig. 10 with coupling constant $\xi = 30$.

ponents $-g_{tt}g_{rr}$ (in area r -coordinates) which differs from one outside the star. This product is actually lower than one at the surface of stars, as shown in Fig. 14.⁷

VI. DISCUSSION

Our results are consistent with those reported in Refs. [39, 40], except that those authors do not study the dynamical transition to SC, but rather obtain the scalarized configurations by solving the field equations in a completely static [39] or stationary (slow rotation) [40] scenarios, and find the non trivial scalar field configuration that vanishes asymptotically. In principle, those configurations would correspond

⁷ We construct stellar models in the EF such that $\tilde{g}_{rr} = 1$ in $r = 0$. Transformation to the JF induces $g_{rr} < 1$ in $r = 0$ for scalarized stars.

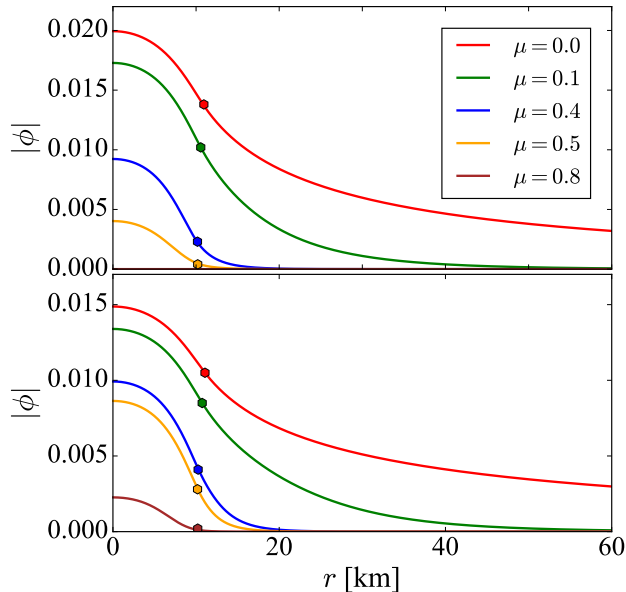


FIG. 12: Scalar-field radial profiles of static configurations consistent with the final state of evolutions shown in Figs. 10 and 11. Top (bottom) panel corresponds to $\xi = 15$ ($\xi = 30$). Colored points indicate stellar radii. As the value of μ increases, the scalar field profiles get suppressed at shorter distances.

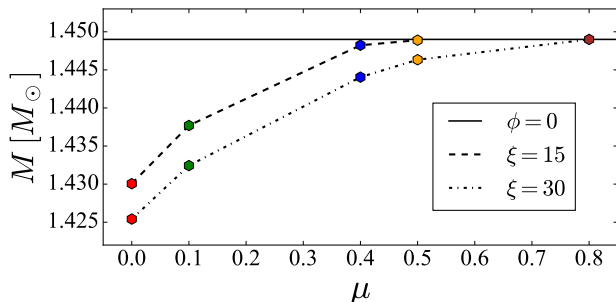


FIG. 13: Total mass M as a function of the scalar-field mass μ , for the end-state of the dynamical processes of scalarization shown in Figs. 10 and 11. The solid, horizontal line indicates the corresponding mass of a (GR) unscalarized star.

approximately to the ones reported here after evolution. But this is not exactly so, because the theory in Refs. [39, 40] is *not* the quadratic NMC STT that we use here. Furthermore, they perform the analysis in the EF with an exponential conformal factor which does not map to the JF theory used here. However, the most important point to stress is that, in principle, the suppression of the scalar field is such that one avoids the bounds imposed by the binary systems on the value of ξ , notably by PSR J0348+0432 [29] because the scalar field be-

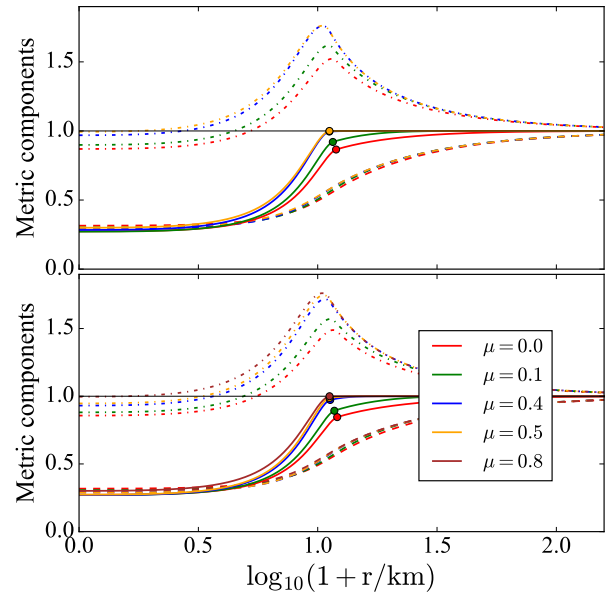


FIG. 14: Metric components of spacetimes consistent with the endpoint of evolutions shown in Figs. 10 and 11, in the cases of $\xi = 15$ (top panel) and $\xi = 30$ (bottom panel). Dashed lines correspond to $-g_{tt}$, dotted lines to g_{rr} , and solid lines to the product $-g_{tt}g_{rr}$. Circles indicate stellar surfaces.

comes short-ranged and would not have a noticeable effect on the companion, which orbits around 10^7 km away from the scalarized NS, and also because possible GW-dipole radiation is also suppressed by the mass term [55]. This length scale of the binary system orbit translates into a mass $\mu \gg 10^{-16}$ eV [39] in order to avoid the observational bounds.⁸ At the same time, one would expect the scalarization effects to be large enough so that SC leaves a trace that can be detected in some way, like by suitable detectors of a breathing mode of scalar waves during the scalarization transition, or as a trace in the GW signal emitted, for instance, during binary NS mergers. This implies that the mass term should be small enough to avoid a total suppression of the scalarization effects inside NSs. If one takes the range of the scalar field to be larger than the NS radius ~ 10 km, this translates into $\mu \lesssim 10^{-9}$ eV [39]. Thus, the range allowed for the mass becomes roughly 10^{-16} eV $\ll \mu \lesssim 10^{-9}$ eV. Finally, as argued in [39], the scalar-field mass can be further restricted due to high-spin superradiance effects in stellar-mass black holes [56–58] to be outside the range 10^{-13} eV $\lesssim \mu \lesssim 10^{-11}$ eV. All these bounds lead us, for instance, to explore the mass μ in the domain 10^{-12} eV $\lesssim \mu \lesssim 10^{-9}$ eV which is consistent with the range of masses specified in Sec. II. In practice, this exploration shows that taking $\xi = 15$ the scalar field is practically con-

⁸ In this section, we recover the units of μ , as indicated in Sec. II.

finned within the star for $10^{-9}\text{eV} \lesssim \mu$, while for $\mu \lesssim 10^{-12}\text{eV}$ the scalar field behaves as if it were massless. These remarks can be appreciated in Fig. 12.

Another important difference with respect to the analyses of [39, 40] is that their maximum mass configurations for scalarized static or stationary NSs are completely unavailable from initial data starting from unscalarized NSs (*i.e.* NSs in GR) for a given EOS. These remarks can be better appreciated from Fig. 13, where the larger the NMC constant ξ for a given mass μ and fixed EOS, the lower the gravitational mass, relative to GR, is found at the end of the dynamical scalarization process. This is at odds when one builds stationary NS configurations not from a dynamical process but starting from the structure equations in static situations, for instance. In that case, and as emphasized above, one can build scalarized NS configurations with a larger gravitational mass when increasing ξ (cf. Ref.[28]). In fact, by constructing static scalarized NSs in this way, and above the maximum baryon mass allowed in GR, one cannot even compare NS configurations using energetic arguments. In this sense, while maximum mass models of scalarized NSs above those of GR are interesting in many respects (they might explain the “supermassive” NSs observed recently with masses above $2M_{\odot}$ without the need of an *ad-hoc* EOS, see Ref. [47]) they are unavailable from a dynamical-process point of view, like the one analyzed here since, as we have stressed, *a priori* they cannot be obtained from GR initial data by definition. Again, this is because scalarized NSs always have a mass lower than the initial GR configuration that one started from after the dynamical transition, for a fixed total baryon mass.

A final technical point is in order. In the massless scalar field scenario one computes the *scalar charge* of the star (analogue to magnetization in ferromagnets at low temperatures, which is the order parameter) by an integral that measures the *flux* of the gradient of the scalar field through a two-dimensional sphere at (spatial) infinity (cf. Eq.(7) of Ref.[47]). However, if one uses the same definition in the massive case, then the scalar charge vanishes due to the exponential fall-off of the field away from the star. This situation is similar to a scenario where the photon is massive, in which case, the electric charge of a point-source would vanish far away from the source due to the Yukawa fall-off of the electrostatic potential. Of course, operationally, one can still assign a value to the scalar charge as the coefficient of such a Yukawa term. However, by doing so, one would argue if such a value is a coordinate independent quantity, which does not seem evident *a priori*. Therefore, in the massive case it remains to analyze if the scalar charge thus “defined” operationally is indeed a good measure of the scalarization strength.

VII. CONCLUSIONS

Following our previous numerical analysis about the dynamical transition to scalarized NSs in STT for a massless scalar field, and with a quadratic NMC to the Ricci curvature in the JF [47], we perform here a similar analysis by adding a mass term in order to study its impact on the dynamics. Con-

trary to the massless scenario, the NMC constant ξ can avoid the bounds imposed by several observations in binary systems since the mass term can suppress the range of the scalar field outside the star for a sufficiently large μ , which is still far below the mass of any of the massive particles detected so far within the standard model of particle physics. Our results are consistent with previous studies [39, 40] where the scalarization process with a mass term was analyzed non dynamically, but differ drastically from them in that the initial available energy (the ADM mass) leading to scalarized neutron stars is always, and by definition, larger than the gravitational mass of the final scalarized stationary star at the end of the process, where the energy difference is radiated away in the form of scalar GWs. It is worth investigating if despite the scalar field suppression that allows the avoidance of available bounds with large values of the NMC constant ξ , the field still has some impact on other observational channels, like in GW signals from NS mergers observed by the present and future detectors, such as LIGO-VIRGO-KAGRA, the Einstein Telescope, and LISA.

Acknowledgments

We acknowledge financial support through the CONAH-CyT grant “Ciencia de Frontera” 140630, and Network Projects No. 376127 “Sombras, lentes y ondas gravitatorias generadas por objetos compactos astrofísicos”, and No. 304001 “Estudio de campos escalares con aplicaciones en cosmología y astrofísica”. We also benefited from UNAM-PAPIIT grants IA101123, IN110523, and IN105223, and by the European Horizon Europe staff exchange (SE) programme HORIZON-MSCA2021-SE-01 Grant No. NewFun-FiCO101086251. Numerical simulations were performed at the LAMOD facility at ICN, UNAM.

Appendix A: Transformation between Einstein and Jordan frames

Consider the action of a STT formulated in the Jordan Frame [20],

$$S[g_{ab}; \phi; \psi_m] = \frac{1}{2\kappa} \int [F(\phi)R - Z(\phi)(\nabla\phi)^2 - V(\phi)] \sqrt{-g}d^4x + S_m[g_{ab}; \psi_m], \quad (\text{A1})$$

where F , Z , and V are given functions of the scalar field ϕ , $(\nabla\phi)^2 = g^{ab}\nabla_a\phi\nabla_b\phi$, $\kappa = 8\pi$, and S_m is the action for matter fields ψ_m .

We assume a conformal rescaling of the metric, $g_{ab} = a(\tilde{\phi})^2\tilde{g}_{ab}$, with a function $a(\tilde{\phi})$ of a scalar field $\tilde{\phi}$ related to ϕ through some function $\tilde{\phi}(\phi)$ —see the details below. The metric \tilde{g}_{ab} is known as the *Einstein-frame metric*. Under these assumptions, transforming the action (A1) into the Einstein frame,

$$S[\tilde{g}_{ab}; \tilde{\phi}; \psi_m] = \frac{1}{2\kappa} \int [\tilde{R} - 2(\tilde{\nabla}\tilde{\phi})^2 - \tilde{V}(\tilde{\phi})] \sqrt{-\tilde{g}}d^4x$$

$$+ S_m[\tilde{g}_{ab}; \psi_m], \quad (\text{A2})$$

demands

$$a(\tilde{\phi})^2 = F(\phi(\tilde{\phi}))^{-1}, \quad (\text{A3})$$

$$\tilde{V}(\tilde{\phi}) = F(\phi(\tilde{\phi}))^{-2} V(\phi(\tilde{\phi})), \quad (\text{A4})$$

$$\frac{d\tilde{\phi}}{d\phi} = \sqrt{\frac{3}{4} \left(\frac{F'(\phi)}{F(\phi)} \right)^2 + \frac{Z(\phi)}{2F(\phi)}}. \quad (\text{A5})$$

In the particular case of the action in Eq. (1), we have

$$a(\tilde{\phi}) = \frac{1}{\sqrt{1 + \kappa\xi\phi(\tilde{\phi})^2}}, \quad (\text{A6})$$

$$\tilde{V}(\tilde{\phi}) = \frac{2\kappa}{[1 + \kappa\xi\phi(\tilde{\phi})^2]^2} V(\phi(\tilde{\phi})), \quad (\text{A7})$$

$$\frac{d\tilde{\phi}}{d\phi} = \frac{\sqrt{\kappa/2}}{1 + \kappa\xi\phi^2} \sqrt{1 + \kappa\xi(1 + 6\xi)\phi^2}. \quad (\text{A8})$$

We invert numerically the integral of Eq. (A8), $\tilde{\phi}(\phi)$, in order to recover the scalar field in the Jordan Frame, $\phi(\tilde{\phi})$, which is required to evaluate the functions (A6) and (A7).

Appendix B: Evolution equations

The Einstein-Scalar-field system resulting from variation of the *Einstein frame* action (A2) is

$$\tilde{G}_{ab} - 2\tilde{\nabla}_a\tilde{\phi}\tilde{\nabla}_b\tilde{\phi} + \tilde{g}_{ab}\tilde{\nabla}_c\tilde{\phi}\tilde{\nabla}^c\tilde{\phi} = 8\pi\alpha^2 T_{ab}^{\text{fluid}}, \quad (\text{B1})$$

$$\tilde{\nabla}^a\tilde{\nabla}_b\tilde{\phi} = -4\pi\alpha^4 \alpha T_{\text{fluid}}, \quad (\text{B2})$$

where $\alpha = d \ln a(\tilde{\phi})/d\tilde{\phi}$, and $T_{\text{fluid}} = g_{ab}T_{\text{fluid}}^{ab}$. We consider the spherically symmetric line element in Schwarzschild-like coordinates as

$$d\tilde{s}^2 = -\tilde{N}(t, r)^2 dt^2 + \tilde{A}(t, r)^2 dr^2 + r^2 (d\vartheta^2 + \sin^2\vartheta d\varphi^2), \quad (\text{B3})$$

and we write the evolution equations from (B1)–(B2) collectively with the hydrodynamic equations (16)–(17) as a first-order system of conservation laws,

$$\frac{\partial}{\partial t}(\tilde{A}\mathbf{q}) + \frac{1}{r^2} \frac{\partial}{\partial r} (\tilde{N}\tilde{A}r^2\mathbf{F}(\mathbf{q})) = \mathbf{S}(\mathbf{q}), \quad (\text{B4})$$

where $\mathbf{q} = (D, S, \tau, \eta, \psi)^T$ includes conservative fluid quantities measured by Eulerian observers: baryon-mass density D , radial momentum density S , and internal energy-density τ , defined by

$$D := \rho\Gamma, \quad (\text{B5})$$

$$S := (E + p)A^2v, \quad (\text{B6})$$

$$\tau := E - D, \quad (\text{B7})$$

where $\Gamma = (1 - \tilde{A}^2v^2)^{-1/2}$ is the Lorentz factor, $\tilde{A}v$ is the fluid's radial velocity, and $E = \Gamma^2(\epsilon + p) - p$ is the total energy-density, all of them measured by Eulerian observers. The scalar field variables in \mathbf{q} are defined by

$$\eta := \frac{1}{\tilde{A}} \frac{\partial\tilde{\phi}}{\partial r}, \quad \psi := \frac{1}{\tilde{N}} \frac{\partial\tilde{\phi}}{\partial t}. \quad (\text{B8})$$

The flux and source vectors in Eq. (B4) are, respectively,

$$\mathbf{F}(\mathbf{q}) = (F_D, F_S, F_\tau, F_\eta, F_\psi)^T, \quad (\text{B9})$$

$$\mathbf{S}(\mathbf{q}) = (S_D, S_S, S_\tau, S_\eta, S_\psi)^T, \quad (\text{B10})$$

with

$$F_D = Dv, \quad (\text{B11})$$

$$F_S = Sv + p, \quad (\text{B12})$$

$$F_\tau = (\tau + p)v, \quad (\text{B13})$$

$$F_\eta = -\psi/A, \quad (\text{B14})$$

$$F_\psi = -\eta/A, \quad (\text{B15})$$

and

$$S_D = -3\alpha\tilde{N}\tilde{A}D(\psi + \tilde{A}v\eta), \quad (\text{B16})$$

$$\begin{aligned} S_S = & 2\tilde{N}\tilde{A}\frac{p}{r} - \tilde{N}\tilde{A}^3\frac{\tilde{m}}{r^2}(D + \tau + Sv + p) \\ & - 4\alpha\tilde{N}\tilde{A}\psi S - \alpha\tilde{N}\tilde{A}^2\eta(D + \tau + 3Sv + p) \\ & - \frac{1}{2}\tilde{N}\tilde{A}^3r(\eta^2 + \psi^2)(D + \tau - Sv - p) \\ & + \frac{1}{4}\tilde{N}\tilde{A}^3\tilde{V}r(D + \tau + Sv + p), \end{aligned} \quad (\text{B17})$$

$$\begin{aligned} S_\tau = & -\tilde{N}\tilde{A}S\frac{\tilde{m}}{r^2} - \alpha\tilde{N}\tilde{A}\psi(3\tau + Sv + 3p) \\ & - \alpha\tilde{N}\tilde{A}^2\eta v(D + 4(\tau + p)) - \tilde{N}\tilde{A}^2r\psi\eta(Sv + p) \\ & - \frac{1}{2}\tilde{N}\tilde{A}Sr(\eta^2 + \psi^2 - \tilde{V}/2), \end{aligned} \quad (\text{B18})$$

$$S_\eta = -2\tilde{N}\frac{\psi}{r}, \quad (\text{B19})$$

$$S_\psi = -4\pi\alpha\alpha^4\tilde{N}\tilde{A}(D + \tau - Sv - 3p) - \frac{1}{4}\tilde{N}\tilde{A}\frac{d\tilde{V}}{d\tilde{\phi}}, \quad (\text{B20})$$

where $\tilde{m}(t, r)$ is defined such that $\tilde{A}(t, r) = [1 - 2\tilde{m}(t, r)/r]^{-1/2}$. This mass aspect function evolves according to

$$\frac{\partial\tilde{m}}{\partial t} = r^2\frac{\tilde{N}}{\tilde{A}^2}(\tilde{A}\eta\psi - 4\pi\alpha^4S). \quad (\text{B21})$$

Moreover, at each time step, we enforce the lapse condition

$$\frac{\partial\tilde{N}}{\partial r} = \tilde{A}^2\tilde{N}\left[\frac{\tilde{m}}{r^2} + 4\pi r\alpha^4(Sv + p) + \frac{r}{2}(\eta^2 + \psi^2 - \tilde{V}/2)\right]. \quad (\text{B22})$$

Finally, the baryonic mass is given by

$$M_b = \int_0^{R_s} 4\pi r^2 D a(\tilde{\phi})^3 (1 - 2\tilde{m}/r)^{-1/2} dr. \quad (\text{B23})$$

In the massless case, the evolution system above reduces to the one of Ref. [48].

- [1] T. Damour and G. Esposito-Farese, “Tensor multiscalar theories of gravitation,” *Class. Quant. Grav.* **9**, 2093–2176 (1992).
- [2] Y. Fujii and K.-i. Maeda, *The Scalar-Tensor Theory of Gravitation*, Cambridge Monographs on Mathematical Physics (Cambridge University Press, 2003).
- [3] C. Brans and R. H. Dicke, “Mach’s principle and a relativistic theory of gravitation,” *Phys. Rev.* **124**, 925–935 (1961).
- [4] C. H. Brans, “Mach’s Principle and a Relativistic Theory of Gravitation. II,” *Phys. Rev.* **125**, 2194–2201 (1962).
- [5] R. H. Dicke, “Mach’s principle and invariance under transformation of units,” *Phys. Rev.* **125**, 2163–2167 (1962).
- [6] T. J. Broadhurst, R. S. Ellis, D. C. Koo, and A. S. Szalay, “Large scale distribution of galaxies at the galactic poles,” *Nature* **343**, 726–728 (1990).
- [7] M. Morikawa, “Oscillating Universe: The Periodic Redshift Distribution of Galaxies with a Scale 128 H⁻¹ Megaparsecs at the Galactic Poles,” *ApJ* **362**, L37 (1990).
- [8] M. Salgado, D. Sudarsky, and H. Quevedo, “Galactic periodicity and the oscillating G model,” *Phys. Rev. D* **53**, 6771–6783 (1996), arXiv:gr-qc/9606038 .
- [9] M. Salgado, D. Sudarsky, and H. Quevedo, “Has cosmological dark matter been observed?” *Phys. Lett. B* **408**, 69–74 (1997), arXiv:gr-qc/9606039 .
- [10] H. Quevedo, M. Salgado, and D. Sudarsky, “The oscillating G model: A possible explanation for the nature of cosmological nonbaryonic matter,” *Astrophys. J.* **488**, 14–26 (1997).
- [11] B. Boisseau, G. Esposito-Farese, D. Polarski, and A. A. Starobinsky, “Reconstruction of a scalar tensor theory of gravity in an accelerating universe,” *Phys. Rev. Lett.* **85**, 2236 (2000), arXiv:gr-qc/0001066 .
- [12] L. Amendola, “Dark energy and the Boomerang data,” *Phys. Rev. Lett.* **86**, 196–199 (2001), arXiv:astro-ph/0006300 .
- [13] A. Riazuelo and J.-P. Uzan, “Cosmological observations in scalar - tensor quintessence,” *Phys. Rev. D* **66**, 023525 (2002), arXiv:astro-ph/0107386 .
- [14] C. Schmid, J.-P. Uzan, and A. Riazuelo, “Weak lensing in scalar-tensor theories of gravity,” *Phys. Rev. D* **71**, 083512 (2005), arXiv:astro-ph/0412120 .
- [15] E. E. Flanagan, “The Conformal frame freedom in theories of gravitation,” *Class. Quant. Grav.* **21**, 3817 (2004), arXiv:gr-qc/0403063 .
- [16] M. Salgado, “The Cauchy problem of scalar tensor theories of gravity,” *Class. Quant. Grav.* **23**, 4719–4742 (2006), arXiv:gr-qc/0509001 .
- [17] M. Salgado, D. Martinez-del Rio, M. Alcubierre, and D. Núñez, “Hyperbolicity of scalar-tensor theories of gravity,” *Phys. Rev. D* **77**, 104010 (2008), arXiv:0801.2372 [gr-qc] .
- [18] E. Berti *et al.*, “Testing General Relativity with Present and Future Astrophysical Observations,” *Class. Quantum Grav.* **32**, 243001 (2015), arXiv:1501.07274 [gr-qc] .
- [19] T. Damour and G. Esposito-Farèse, “Nonperturbative strong-field effects in tensor-scalar theories of gravitation,” *Phys. Rev. Lett.* **70**, 2220–2223 (1993).
- [20] T. Damour and G. Esposito-Farese, “Tensor - scalar gravity and binary pulsar experiments,” *Phys. Rev. D* **54**, 1474–1491 (1996), arXiv:gr-qc/9602056 .
- [21] LIGO-Virgo-KAGRA Publications .
- [22] H. Sotani and K. D. Kokkotas, “Stellar oscillations in scalar-tensor theory of gravity,” *Phys. Rev.* **D71**, 124038 (2005), gr-qc/0506060 .
- [23] J. Novak, “Neutron star transition to strong scalar field state in tensor scalar gravity,” *Phys. Rev. D* **58**, 064019 (1998), arXiv:gr-qc/9806022 .
- [24] J. Novak, “Spherical neutron star collapse toward a black hole in a tensor-scalar theory of gravity,” *Phys. Rev. D* **57**, 4789–4801 (1998).
- [25] A. W. Whinnett, “Spontaneous scalarization and boson stars,” *Phys. Rev. D* **61**, 124014 (2000), arXiv:gr-qc/9911052 .
- [26] M. Alcubierre, J. C. Degollado, D. Núñez, M. Ruiz, and M. Salgado, “Dynamic transition to spontaneous scalarization in boson stars,” *Phys. Rev.* **D81**, 124018 (2010), arXiv:1003.4767 [gr-qc] .
- [27] D. D. Doneva, F. M. Ramazanoğlu, H. O. Silva, T. P. Sotiriou, and S. S. Yazadjiev, “Spontaneous scalarization,” *Rev. Mod. Phys.* **96**, 015004 (2024), arXiv:2211.01766 [gr-qc] .
- [28] M. Salgado, D. Sudarsky, and U. Nucamendi, “Spontaneous scalarization,” *Phys. Rev. D* **58**, 124003 (1998).
- [29] J. Antoniadis *et al.*, “A Massive Pulsar in a Compact Relativistic Binary,” *Science* **340**, 6131 (2013), arXiv:1304.6875 [astro-ph.HE] .
- [30] P. Demorest, T. Pennucci, S. Ransom, M. Roberts, and J. Hessels, “A two-solar-mass neutron star measured using Shapiro delay,” *Nature* **467**, 1081–1083 (2010), arXiv:1010.5788 [astro-ph.HE] .
- [31] H. T. Cromartie *et al.* (NANOGrav), “Relativistic Shapiro delay measurements of an extremely massive millisecond pulsar,” *Nature Astron.* **4**, 72–76 (2019), arXiv:1904.06759 [astro-ph.HE] .
- [32] R. W. Romani, D. Kandel, A. V. Filippenko, T. G. Brink, and W. Zheng, “PSR J0952–0607: The Fastest and Heaviest Known Galactic Neutron Star,” *Astrophys. J. Lett.* **934**, L17 (2022), arXiv:2207.05124 [astro-ph.HE] .
- [33] P. C. C. Freire *et al.*, “The relativistic pulsar-white dwarf binary PSR J1738+0333 - II. The most stringent test of scalar-tensor gravity,” *Mon. Not. Roy. Astron. Soc.* **423**, 3328 (2012), arXiv:1205.1450 [astro-ph.GA] .
- [34] L. Shao, N. Sennett, A. Buonanno, M. Kramer, and N. Wex, “Constraining nonperturbative strong-field effects in scalar-tensor gravity by combining pulsar timing and laser-interferometer gravitational-wave detectors,” *Phys. Rev. X* **7**, 041025 (2017), arXiv:1704.07561 [gr-qc] .
- [35] M. Kramer *et al.*, “Strong-Field Gravity Tests with the Double Pulsar,” *Phys. Rev. X* **11**, 041050 (2021), arXiv:2112.06795 [astro-ph.HE] .
- [36] J. Zhao, P. C. C. Freire, M. Kramer, L. Shao, and N. Wex, “Closing a spontaneous-scalarization window with binary pulsars,” *Class. Quant. Grav.* **39**, 11LT01 (2022), arXiv:2201.03771 [astro-ph.HE] .
- [37] R. F. P. Mendes and T. Ottoni, “Scalar charges and pulsar-timing observables in the presence of nonminimally coupled scalar fields,” *Phys. Rev. D* **99**, 124003 (2019), arXiv:1903.11638 [gr-qc] .
- [38] P. Chen, T. Suyama, and J. Yokoyama, “Spontaneous-scalarization-induced dark matter and variation of the gravitational constant,” *Phys. Rev. D* **92**, 124016 (2015).
- [39] F. M. Ramazanoğlu and F. Pretorius, “Spontaneous Scalarization with Massive Fields,” *Phys. Rev. D* **93**, 064005 (2016), arXiv:1601.07475 [gr-qc] .
- [40] S. S. Yazadjiev, D. D. Doneva, and D. Popchev, “Slowly rotating neutron stars in scalar-tensor theories with a massive scalar field,” *Phys. Rev. D* **93**, 084038 (2016), arXiv:1602.04766 [gr-qc] .

- [41] D. D. Doneva and S. S. Yazadjiev, “Rapidly rotating neutron stars with a massive scalar field—structure and universal relations,” *JCAP* **11**, 019 (2016), arXiv:1607.03299 [gr-qc] .
- [42] U. Sperhake, C. J. Moore, R. Rosca, M. Agathos, D. Gerosa, and C. D. Ott, “Long-lived inverse chirp signals from core collapse in massive scalar-tensor gravity,” *Phys. Rev. Lett.* **119**, 201103 (2017), arXiv:1708.03651 [gr-qc] .
- [43] K. V. Staykov, D. Popchev, D. D. Doneva, and S. S. Yazadjiev, “Static and slowly rotating neutron stars in scalar-tensor theory with self-interacting massive scalar field,” *Eur. Phys. J. C* **78**, 586 (2018), arXiv:1805.07818 [gr-qc] .
- [44] R. Rosca-Mead, C. J. Moore, U. Sperhake, M. Agathos, and D. Gerosa, “Structure of neutron stars in massive scalar-tensor gravity,” *Symmetry* **12**, 1384 (2020), arXiv:2007.14429 [gr-qc] .
- [45] H.-J. Kuan, K. Van Aelst, A. T.-L. Lam, and M. Shibata, “Binary neutron star mergers in massive scalar-tensor theory: Quasiequilibrium states and dynamical enhancement of the scalarization,” *Phys. Rev. D* **108**, 064057 (2023), arXiv:2309.01709 [gr-qc] .
- [46] A. T.-L. Lam, H.-J. Kuan, M. Shibata, K. Van Aelst, and K. Kiuchi, “Binary neutron star mergers in massive scalar-tensor theory: Properties of post-merger remnants,” (2024), arXiv:2406.05211 [gr-qc] .
- [47] J. C. Degollado, M. Salgado, and M. Alcubierre, “On the formation of “supermassive” neutron stars and dynamical transition to spontaneous scalarization,” *Phys. Lett. B* **808**, 135666 (2020), arXiv:2008.10683 [gr-qc] .
- [48] R. F. P. Mendes and N. Ortiz, “Highly compact neutron stars in scalar-tensor theories of gravity: Spontaneous scalarization versus gravitational collapse,” *Phys. Rev. D* **93**, 124035 (2016), arXiv:1604.04175 [gr-qc] .
- [49] M. Ruiz, J. C. Degollado, M. Alcubierre, D. Núñez, and M. Salgado, “Induced scalarization in boson stars and scalar gravitational radiation,” *Phys.Rev.* **D86**, 104044 (2012), arXiv:1207.6142 [gr-qc] .
- [50] B. Bertotti, L. Iess, and P. Tortora, “A test of general relativity using radio links with the Cassini spacecraft,” *Nature* **425**, 374–376 (2003).
- [51] S. Ma, V. Varma, L. C. Stein, F. Foucart, M. D. Duez, L. E. Kidder, H. P. Pfeiffer, and M. A. Scheel, “Numerical simulations of black hole-neutron star mergers in scalar-tensor gravity,” *Phys. Rev. D* **107**, 124051 (2023), arXiv:2304.11836 [gr-qc] .
- [52] R. F. P. Mendes, N. Ortiz, and N. Stergioulas, “Nonlinear dynamics of oscillating neutron stars in scalar-tensor gravity,” *Phys. Rev. D* **104**, 104036 (2021), arXiv:2107.07036 [gr-qc] .
- [53] M. Alcubierre, J. Barranco, A. Bernal, J. C. Degollado, A. Diez-Tejedor, M. Megevand, D. Núñez, and O. Sarbach, “Dynamical evolutions of ℓ -boson stars in spherical symmetry,” *Class. Quant. Grav.* **36**, 215013 (2019), arXiv:1906.08959 [gr-qc] .
- [54] R. F. P. Mendes and N. Ortiz, “New class of quasinormal modes of neutron stars in scalar-tensor gravity,” *Phys. Rev. Lett.* **120**, 201104 (2018), arXiv:1802.07847 [gr-qc] .
- [55] J. Alsing, E. Berti, C. M. Will, and H. Zaglauer, “Gravitational radiation from compact binary systems in the massive Brans-Dicke theory of gravity,” *Phys. Rev. D* **85**, 064041 (2012), arXiv:1112.4903 [gr-qc] .
- [56] V. Cardoso, I. P. Carucci, P. Pani, and T. P. Sotiriou, “Black holes with surrounding matter in scalar-tensor theories,” *Phys. Rev. Lett.* **111**, 111101 (2013), arXiv:1308.6587 [gr-qc] .
- [57] R. Brito, V. Cardoso, and P. Pani, “Black holes as particle detectors: evolution of superradiant instabilities,” *Class. Quant. Grav.* **32**, 134001 (2015), arXiv:1411.0686 [gr-qc] .
- [58] R. Brito, V. Cardoso, and P. Pani, “Superradiance: New Frontiers in Black Hole Physics,” *Lect. Notes Phys.* **906**, pp.1–237 (2015), arXiv:1501.06570 [gr-qc] .